PWM investigation of a Field-oriented controlled Five-Phase PMSM under two-phase open faults

Bing Tian, Marta Molinas, *Member, IEEE*, Quntao An, *Member, IEEE*

***Abstract*-- The decoupled model of Five-Phase Permanent Magnet Synchronous Motors (5Ph PMSMs) under a two-phase open circuit has been developed recently, yet the corresponding PWM has not been fully exploited. The Pulse Width Modulation (PWM), which is straightforward for a balanced system, can be problematic to fit a 5Ph PMSM under faulty conditions. During the open faults, the neutral voltage is drifting over the mid-point of DC bus, thus, the PWM typically designed for a balanced system always fails. In this paper, an affine transformation is first presented to offset the drifting neutral effect, and only then PWMs can be effective. A quasi-sinusoidal PWM, a Space Vector PWM, and a min-max Carrier-based PWM are presented and compared experimentally. Each method has its own merits and demerits, and their effectiveness or rather the proposed affine transformation is validated by the experimental results.**

***Index Terms*—Min-max CBPWM, SVPWM, Drifting Neutral, Five-phase PMSM, Two-phase open fault.**

I. Introduction

Multi-phase machines are replacing the three-phase (3Ph) drive in some safety crucial applications because of high power density, high reliability, and excellent fault-tolerant capacities[1, 2]. Therefore, the fault-tolerant operation of a multiphase motor after losing one or more phases has received tremendous attention. Normally, by maintaining an equivalent (not the related) rotating fundamental Magnetomotive Force (MMF) as before the fault, the multiphase machine can still operate steadily[3, 4]. As it suggests, a controllable MMF can be significant for the convenience of derating operation during the post fault. The fault types can be grouped into the short circuit and open circuit faults. However, the short circuit leads to the motor overheating and even causes irreversible secondary damage to the permanent magnet, and, thus, this type of fault is always transformed to an open circuit fault in its earlier occurrence via quick fuses [5]. In other words, the research on the open fault-tolerant control (FTC) is of remarkable importance to enhance motor reliability in the event of certain failures.

The FTC of multiphase motors is of a high-level searching algorithm for the optimal current solutions under, for instance, a minimum torque-ripple constraint, besides preserving a rotating fundamental MMF [6-8]. In [6], the optimal post-fault currents are searched offline using a global closed-form optimal algorithm, and then the motor currents are regulated in a hysteresis manner. In real life, the complexity of FTC may differ from motor to motor. In the early time, the fault-tolerant motor (FTM) is intensively focused, which is subject to the modular design to pursue the magnetic and thermal isolation between phases [9-11]. This type of motor usually has low mutual-inductances, constant self-inductances, and/or sinusoidal back electromotive forces (back-EMFs). Given its simple structure, the post-fault currents are well able to be re-configured at the phase coordinate frame. In [7], a genetic seeking algorithm is presented to solve the optimal current references under the constraint of a minimum torque-ripple, and a flux-switching motor featured by a small mutual-inductance is attempted experimentally. On the other hand, the optimal current solutions are sometimes too idealized to fit a real drive. A. Mohammadpour, [6], concludes that the desired torque-ripple free is somehow not fully achieved in reality, and this problem is probably caused by the truth that the FTM is more complex than expected. Whereas, in some other applications, *e.g.*, propulsion systems and electric vehicles, the motor involved demands to have a very compact structure and a higher power density. In these cases, a trapezoidal back-EMF with additional reluctance-torques is appreciated. The FTC of an earlier time lacks compatibility among different model types. In [12], the FTC of a trapezoidal back-EMF Five-Phase Permanent Magnet Synchronous Motors (5Ph PMSM) is attempted, and the optimal current solution is solved offline under the constraint of ripple-free electromagnetic power. However, only the hysteresis regulator can be applied, and this method is incapable of being extended to other motor types because of the ill-consideration of the armature reaction. The post-fault current re-configuration of a trapezoidal back-EMF motor can be quite involved under the

stationary phase coordinate frame. To cope with this issue, the transformation of the faulty motor model to the rotor-oriented frame seems more appealing. Hugo Guzman, [13], presents a vector control for a 5Ph fault-tolerant induction motor under a single-phase open fault such that the post-fault currents can be solved conveniently under the d-q frame. Encouraged by this result, [14] develops a decoupled model for a generic 5Ph PMSM also under a single-phase open fault. Huawei Zhou, [15], proposes a set of Clarke and Park transformations for the field-oriented control (FOC) of an FTM under a single-phase open fault, and as the title implies this FOC is only applicable to a certain motor type with constant self-inductances and negligible mutual-inductances. Luming Chen, [16], presents a post-fault decoupling vector control for a 5Ph PMSM under a single-phase open fault, however, the rotor-flux and inductance matrices of the developed model remains time-variant. Recently, the decoupled models for a 5Ph PMSM under two-phase open faults have also been established [17], and it suggests that the FOC in this fault mode is also possible.

Despite the above attempts to regulate the MMF under the *d-q* frame, the post-fault operation is still problematic because of the drifting neutral [18, 19]. Basically, the post-fault operation of a multi-phase drive is comprised of three layers: (1) the outer-layer FTC, which calculates an optimal current online or offline under certain constraints; (2) the inner-layer current regulators, of which the references are given by the FTC; and (3) the inner-most layer PWM techniques, which are responsible for the correct modulation of phase voltages. Foremost among them, the PWM constitutes the most fundamental part of an inverter-driven system. Even though the PWM is quite simple and straightforward for a balanced 3Ph/5Ph system, it can be problematic to fit a motor drive under faulty conditions. For a 5Ph-PMSM with one- or two-phase open-circuited, the neutral voltage is shifting relative to the potential of mid-point of DC bus, and this condition poses a challenge for PWM implementation.

Commonly, the PWM approaches for a FOC-based motor drive can be categorized as 1) Sinusoidal Pulse Width Modulation (SPWM), 2) Space Vector PWM (SVPWM), and 3) the up-to-date Carrier-Based PWM (CBPWM) [20]. The SVPWM is well known for its high DC bus utilization and low switching losses and, thus, it has gained tremendous attention in the last few decades [21]. Recently, this sophisticated SVPWM is being replaced by a min-max CBPWM featured by certain common-mode voltage (CMV) injection and an identical output performance with the classical SVPWM. Even though the universal validity of this min-max CBPWM has been justified in the previous literature, regardless of the phase number and load conditions [20, 22, 23]. But until now, there are still no relevant articles to reveal how to implement this CBPWM into a faulty 5Ph PMSM. This work fills this gap.

During the post-fault operation, the motor experiences a significant power derating, and thus the properties of the high-DC bus utilization and lower switching losses are particularly demanding for 5Ph drives powered by battery packs. Guohai Liu, [24], comparatively investigated two SVPWM strategies for an FTM (having a constant inductance) under a single-phase open fault. However, the drifting neutral effect is somehow neglected. Qian Chen, [25], presents an asymmetrical SVPWM for a fault-tolerant drive under a single-phase open fault, and the drifting neutral on PWM implementation is still not paid enough attention. Hugo Guzman, [11], incorporates this problem into the decoupled modeling of a 5Ph FTM (an induction motor type), but the PWM technique is still obscure concerning the foresaid drifting neutral. Likewise, the drifting neutral is omitted as well in [16] during the implementation of post-fault vector control for a 5Ph PMSM under a single-phase open fault. Finally, the drifting neutral is stressed again in [19] during the implementation of SVPWM-based direct torque control (DTC) for a 5Ph FTM under a single-phase open fault. The above article centers on a simple extension of three-phase SVPWM to the faulty 5Ph drive with space voltage synthesis performed on α-β-α_3-β_3 plane. However, this method causes some confusion about the vector decomposition as this faulty 5Ph has only 3 degrees of freedom (DOFs) available. To gain a better understanding of the feasible DOFs of a practical drive, it is worthwhile to recall that an *n*-phase system can be only be split into ½(*n*-1) linearly independent 2-D planes for the decoupling control [26]. To be specific, a 5Ph system can be partitioned into two mutually perpendicular 2-D planes [27, 28]; and a 4Ph system can be divided into one 2-D plane for the first harmonic decoupling and one half 2-D plane for third harmonic decoupling [14, 29, 30]; whereas a 3Ph system possesses only one 2-D plane.

Despite several other pieces of research investigating the SVPWM of 5Ph drives under a single-phase open fault, a feasible PWM technique under two-phase open faults is rarely reported. The feasible PWMs rely on the referenced decoupled model. In [17], the FOC of 5Ph PMSMs under the two-phase open fault is theoretically resolved by incorporating the open-phase back-EMFs into the decoupled modeling; however, the authors fail to demonstrate how the phase voltage is modulated when the motor neutral voltage drifts over the mid-point of DC bus. In this work, an affine transformation is proposed to mitigate the drifting neutral effect by the real-time estimation of open phase back-EMFs, and only then can the PWMs be applied. Accordingly, three PWM techniques, *i.e.*, a quasi-SPWM (Q-SPWM), an SVPWM, and a min-max CBPWM, are presented and compared experimentally, which validate the effectiveness of the proposed affine transformation to offset the drifting neutral effect.

II. Decoupled Model

In industrial applications, FOC is attractive because the torque and flux can be controlled separately in a similar way as one controls a brush DC motor. The FOC is dependent on the decoupled modeling and for this purpose, the work [17] presented a set of Clarke and Park transformations for the FOC of 5Ph-PMSMs with two phases open-circuited. The open fault type can be classified into adjacent and non-adjacent-phase open-circuited faults, as the FOC philosophy behind them remains the same, the PWM techniques are elaborated with the example of the adjacent-phase open fault.

Without losing generality, assume phase-A and -B are open-circuited, and the decoupled model, in this context, is given by:

$$\begin{bmatrix} u_d \\ u_q \end{bmatrix} = R_s \begin{bmatrix} i_d \\ i_q \end{bmatrix} + \frac{d}{dt}\left(\begin{bmatrix} L_d & 0 \\ 0 & L_q \end{bmatrix} \begin{bmatrix} i_d \\ i_q \end{bmatrix} \right) - \omega \begin{bmatrix} 0 & 1 \\ -1 & 0 \end{bmatrix} \begin{bmatrix} L_d & 0 \\ 0 & L_q \end{bmatrix} \begin{bmatrix} i_d \\ i_q \end{bmatrix} + \omega \psi_{m1} \begin{bmatrix} 0 \\ 0.6 + 0.4\cos\delta \end{bmatrix} \quad (1)$$

where δ is the space angle difference between the adjacent phase winding axes, with $\delta=2\pi/5$; u_d and u_q are d- and q-axis voltages; i_d, i_q are d- and q-axis currents; ω is the motor speed (electrical); ψ_{m1} is the magnitude of first-order rotor fluxes; and L_d and L_q are d- and q-axis inductances given by

$$\begin{aligned} L_d &= L_{ls} + 2.5\left(0.6 + 0.4\cos\delta\right)\left(L_m - L_\theta\right) \\ L_q &= L_{ls} + 2.5\left(0.6 + 0.4\cos\delta\right)\left(L_m + L_\theta\right) \end{aligned} \quad (2)$$

where L_{ls} is the leakage inductance; L_m and L_θ are, respectively, the magnitudes of constant and alternating inductances out of the non-uniform air gap; and L_d and L_q are constant provided the stator windings are sinusoidally distributed.

It should be emphasized here that L_d and L_q are the d-q frame inductances of the fault case, whose values decrease compared to ones in the healthy mode. Recall that in the heathy case, a trapezoidal back-EMF 5Ph PMSM is split into two 2-D planes[27, 28]: *i.e.*, 1) the α-β plane for first harmonic decomposition, and 2) the α_3-β_3 plane for the third harmonic decomposition. Most importantly, these two 2-D planes are linearly independent, and thus, the 5Ph PMSM can be uniquely represented by their linear combination. Under the two-phase open fault, the 5Ph drive has only one α-β plane available for the first harmonic decoupling control, and in this context, the third harmonics are to stay alternating on this plane. Readers may refer to a latter section for the representation of 3rd order rotor fluxes under this d-q frame.

The average torque in this fault case is given by

$$T_e = \frac{5P}{2} \frac{i_d i_q \left(L_d - L_q\right)}{0.6 + 0.4\cos\delta} + \frac{5}{2} P i_q \psi_{m1} \quad (3)$$

where T_e is the electromagnetic torque, and P is the number of pole pairs. In a trapezoidal back-EMF motor, amounts of harmonic torques are produced because of the harmonic rotor fluxes. The harmonic torques are temporarily ignored in (3) since this paper does not involve high-level FTC algorithms.

The Clarke and Park matrices are given as below

$$\left[\mathbf{T}_{\text{clk}}\right] = \frac{2}{5} \begin{bmatrix} \cos 2\delta - \cos\delta & \cos 3\delta - \cos\delta & \cos 4\delta - \cos\delta \\ \sin 2\delta - \tan\frac{\delta}{2}\cos\delta & \sin 3\delta - \tan\frac{\delta}{2}\cos\delta & \sin 4\delta - \tan\frac{\delta}{2}\cos\delta \\ 1 & 1 & 1 \end{bmatrix} \quad (4)$$

$$\left[\mathbf{T}_{\text{prk}}\right] = \begin{bmatrix} \cos\theta & \sin\theta & 0 \\ -\sin\theta & \cos\theta & 0 \\ 0 & 0 & 1 \end{bmatrix} \quad (5)$$

where θ denotes the rotor position (electrical); and $[T_{prk}]$ and $[T_{clk}]$ indicate, respectively, the modified Park and Clarke matrices which are valid for star-connected 5Ph PMSMs only.

Fig.1 refers to the FOC-based FTC for 5Ph-PMSMs under a two-phase open fault. In the figure, $i_{d,ref}$ and $i_{q,ref}$ are the d-q frame reference currents given by the FTC algorithm; $T_{e,ref}$ is the average torque setpoint given by the speed regulator; and PIR stands for the proportional-integral-resonant controller to damp the current harmonics caused by the harmonic winding coils. Notice that the zero-sequence voltage reference, $u_{o,\text{ref}}$, defaults to 0, and it is overridden by a zero-sequence signal in the case of CBPWM. From Fig.1, the advantages of FOC are noticeable, however, it is still problematic to fit the simplest SPWM into the decoupled model in connection with a drifting neutral. This paper attempts to fix this issue.

III. Drifting Neutral And The Proposed Solution

A. Drifting neutral

In the healthy mode, the phase currents are configured with an evenly spaced phase shift and the identical amplitude to form a rotating MMF. In the fault mode, the inactive phases are not powered any longer, and given this fact, the energized windings can be deemed unevenly distributed around the stator yoke. Evidently, the currents of active phases must also be re-configurated in an uneven manner to form the desired MMF, and this optimization problem can be well solved under the FOC. This paper focuses on a more basic topic: how to implement the PWM to better regulate the MMF.

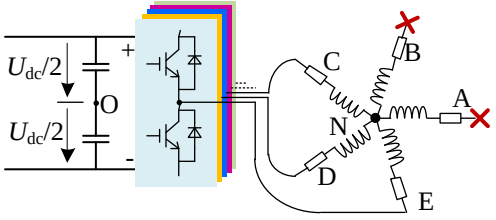

Fig.2 The equivalent circuit of 5Ph-PMSMs with loss of two phases

Fig.2 shows the equivalent circuit of 5Ph-PMSMs with the loss of the excitation in phase-A and -B. From Fig.2, the phase voltages of the energized windings can be represented by [31]

$$\begin{cases} u_{\text{CN}} = u_{\text{CO}} - u_{\text{NO}} \\ u_{\text{DN}} = u_{\text{DO}} - u_{\text{NO}} \\ u_{\text{EN}} = u_{\text{EO}} - u_{\text{NO}} \end{cases} \quad (6)$$

where u_{iN} is the phase voltage (also known as phase-to-neutral voltage) with i=A,B,C,D,E; u_{NO} is the motor neutral voltage

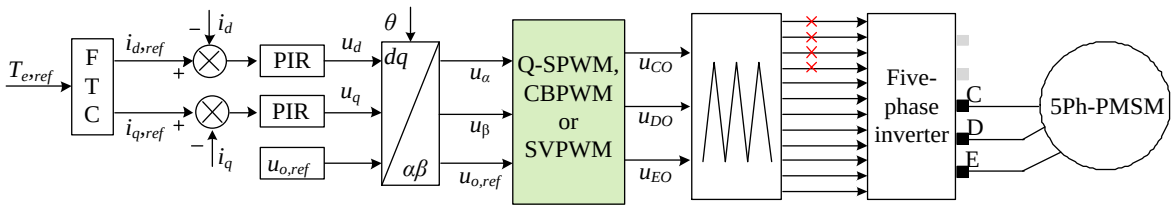

Fig.1 FOC-based FTC for 5Ph PMSM drive under a two-phase open fault.

measured between the neutral point (denoted as "N") and the midpoint of DC bus (denoted as "O"); and u_{xO}, x=*C,D,E*, is the pole voltage measured between the corresponding motor terminal and "O" point. The pole voltages are represented by:

$$\begin{bmatrix} u_{\mathrm{CO}} \\ u_{\mathrm{DO}} \\ u_{\mathrm{EO}} \end{bmatrix} = U_{\mathrm{dc}} \left(\begin{bmatrix} S_{\mathrm{C}} \\ S_D \\ S_E \end{bmatrix} - \frac{1}{2} \begin{bmatrix} 1 \\ 1 \\ 1 \end{bmatrix} \right) \tag{7}$$

where U_{dc} is the DC bus voltage. S_i (i=*C, D, E*) is the switch status of the upper IGBT of each bridge. For simplicity, the switch state vector [**S**] ([**S**]=[S_C S_D S_E]$^{\mathrm{T}}$) is adopted to code the switching sequence.

For a 5Ph-PMSM, there exists (refer to the appendix):

$$u_{AN} + u_{BN} + u_{CN} + u_{DN} + u_{EN} \equiv 0 \tag{8}$$

Substitute (6) and (7) into (8), one can obtain

$$\begin{aligned} u_{NO} &= \frac{1}{3}\left(u_{CO} + u_{DO} + u_{EO}\right) + \frac{1}{3}(u_{AN} + u_{BN}) \\ &= \frac{U_{\mathrm{dc}}}{3}\left(S_C + S_D + S_E\right) - \frac{U_{dc}}{2} + \frac{1}{3}(u_{AN} + u_{BN}) \end{aligned} \tag{9}$$

As per (9), under open faults, u_{NO} is affected by the residual voltages of the inactive phases. In the healthy mode, the phase voltages are deemed identical to the pole voltages so as to simplify the SVPWM implementation. Unfortunately, in the fault mode, this precondition does not hold.

Suppose u_{CN}, u_{DN}, and u_{EN} are the real phase voltages, then the active phase voltages under the α-β frame are given by

$$\begin{bmatrix} u_\alpha & u_\beta & u_o \end{bmatrix}^{\mathrm{T}} = \left[\mathbf{T}_{\mathrm{clk}}\right] \begin{bmatrix} u_{CN} & u_{DN} & u_{EN} \end{bmatrix}^{\mathrm{T}} \tag{10}$$

Combining (6) and (9) with (10) yields the following:

$$\begin{aligned} \begin{bmatrix} u_\alpha \\ u_\beta \\ u_o \end{bmatrix} &= \left[\mathbf{T}_{ploe2xy}\right] \begin{bmatrix} u_{CO} \\ u_{DO} \\ u_{EO} \end{bmatrix} \\ &+ \frac{2(u_{AN} + u_{BN})}{5} \begin{bmatrix} \cos\delta + \dfrac{1+\cos\delta}{3} \\ \tan\dfrac{\delta}{2}\cos\delta + \dfrac{\sin\delta}{3} \\ 0 \end{bmatrix} + \begin{bmatrix} 0 \\ 0 \\ -6/5\, u_{NO} \end{bmatrix} \end{aligned} \tag{11}$$

where [$T_{pole2xy}$] is accordingly defined as

$$\left[\mathbf{T}_{ploe2xy}\right] = \frac{2}{5} \begin{bmatrix} \cos 2\delta + \dfrac{1+\cos\delta}{3} & \cos 3\delta + \dfrac{1+\cos\delta}{3} & \cos 4\delta + \dfrac{1+\cos\delta}{3} \\ \sin 2\delta + \dfrac{\sin\delta}{3} & \sin 3\delta + \dfrac{\sin\delta}{3} & \sin 4\delta + \dfrac{\sin\delta}{3} \\ 1 & 1 & 1 \end{bmatrix} \tag{12}$$

From (11), the voltage vector synthesis is quite difficult to implement because of u_{AN} and u_{BN}. Thus, steps must be taken to mitigate the drifting neutral effect on PWM implementation.

B. The proposed affine transformation

From the foregoing analysis, it can be inferred that voltage compensation with u_{AN} and u_{BN} seems quite helpful to PWM implementation. Therefore, the most effective solution to this problem is resorting to the phase voltage sensing techniques and then trying to offset this drifting neutral effect in a digital signal processor (DSP). However, this approach is impractical since even the open-circuited phase voltage can be like the PWM signal which is difficult to sample. Under Phase-A and -B open fault, phase-A voltage can be represented by:

$$u_{AN} = \frac{d}{dt}\left(L_{AC} i_C + L_{AD} i_D + L_{AE} i_E\right) + e_A \tag{13}$$

where L_{AC}, L_{AD}, L_{AE} are the mutual inductances of Phase-A, e_A is phase-A back-EMF, and i_C, i_D, i_E are the active phase currents. From (13), phase-A voltage comprises not only the back-EMF signal but also some mutually induced EMFs. As the active phase currents are with high-frequency ripples because of the inverter chopping, the time derivative of the ripple is the PWM signal which consequently contaminates eA. Since the motor drive requires speed derating in the event of an open fault, this implies that the EMF due to the mutually induced EMF is much smaller than the back-EMF and thus can be neglected. From now on, u_{AN} and u_{BN} are replaced by e_A and e_B which are shown as below

$$e_A = -\omega\psi_{m1}\sin\theta - 3\omega\psi_{m3}\sin 3\theta \tag{14}$$

$$e_B = -\omega\psi_{m1}\sin\left(\theta - \delta\right) - 3\omega\psi_{m3}\sin\left(3\theta - 3\delta\right) \tag{15}$$

where ψ_{m3} is the magnitude of third harmonic rotor fluxes.

Consequently, a new *x-y* frame, as revealed by (16), is primarily constructed by removing the e_A (u_{AN}) and e_B (u_{BN}) related terms from (11). The relationship between the *x-y* frame voltages and pole voltages can be given by

$$\begin{bmatrix} v_x & v_y & v_{\mathrm{o}} \end{bmatrix}^{\mathrm{T}} = \left[\mathbf{T}_{Ploe2xy}\right] \begin{bmatrix} u_{CO} & u_{CO} & u_{CO} \end{bmatrix}^{\mathrm{T}} \tag{16}$$

where v_x, v_y, v_o are the pole voltages represented under this new *x-y-o* frame. Notice that the use of the *x-y-o* frame is non-related to the commonly used α-β-*x-y*-o coordinate frame that is initially proposed for a healthy 5Ph PMSM.

Substitute (16) into (11), one can have the following equality which contains the proposed affine transformation.

$$\begin{aligned} \begin{bmatrix} v_x \\ v_y \\ v_o \end{bmatrix} &= \begin{bmatrix} 1 & 0 & 0 \\ 0 & 1 & 0 \\ 0 & 0 & 1 \end{bmatrix} \begin{bmatrix} u_\alpha \\ u_\beta \\ u_o \end{bmatrix} - \frac{2(e_{\mathrm{A}} + e_{\mathrm{B}})}{5} \begin{bmatrix} \cos\delta + \dfrac{1+\cos\delta}{3} \\ \tan\dfrac{\delta}{2}\cos\delta + \dfrac{\sin\delta}{3} \\ 0 \end{bmatrix} + \begin{bmatrix} 0 \\ 0 \\ \dfrac{6u_{NO}}{5} \end{bmatrix} \\ &\approx \begin{bmatrix} 1 & 0 & -0.2981 & 0 \\ 0 & 1 & -0.2166 & 0 \\ 0 & 0 & 0 & 1 \end{bmatrix} \begin{bmatrix} u_\alpha \\ u_\beta \\ e_A + e_B \\ u_o + \dfrac{6u_{NO}}{5} \end{bmatrix} \end{aligned} \tag{17}$$

Notice that v_{o} is the sum of pole voltages of the energized windings, while u_o denotes the sum of the remaining healthy phase voltages. Since there is no return path for the zero-sequence current, the zero-sequence voltage can be ignored.

The benefit of having this transformation is that the produced space vectors on this affine plane are time-invariant regardless of motor operation states, and consequently the

voltage vector reference, which shall also be mapped onto the affine plane, has the potential to be synthesized by the basic space vectors. However, it is worth noting that the affine transformation does not preserve the angle before and after the transform and thus sector determination of the SVPWM differs from the traditional one for a balanced system.

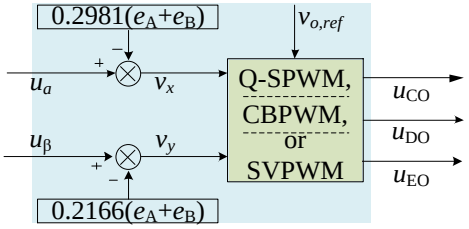

Fig.3 The proposed method to mitigate the drifting neutral effect

The proposed method to mitigate the drifting neutral effect for this unbalanced drive is illustrated in Fig.3. Obviously, the PWM under this scenario is quite different from the one for a balanced system. Based on the affine transformation, the Q-SPWM, the SVPWM, and the up-to-date min-max CBPWM can be applicable which are discussed in a later section.

C. The existing harmonic currents

The decoupled model of (1) can be applied only when the drifting neutral effect is properly incorporated into the inverter modeling. For an FTM with sinusoidally distributed windings, the behavior of the fundamental currents can be, therefore, fully predictable. However, regarding a 5Ph PMSM with trapezoidal distribution windings, the fundamental phase currents can be distorted by some harmonic components. The investigated motor contains certain third harmonic winding constituents which are manifested as third back-EMF as well as additional second and sixth harmonic inductances [27, 28]. In fact, it is difficult to achieve pure sinusoidal distribution of stator winding for most PMSMs, and thus it is meaningful to investigate the principal factors affecting current distortion.

In the fault mode, the third harmonic rotor fluxes are unable to get decoupled from the rotor position and under the *d-q* frame they are represented as:

$$\begin{bmatrix}\tilde{\psi}_{rd}\\ \tilde{\psi}_{rq}\end{bmatrix}=0.2764\psi_{m3}\begin{bmatrix}-\cos(4\theta+0.5\delta)-1.618\cos(2\theta-\delta)\\ \cos(4\theta+0.5\delta)-1.618\cos(2\theta-\delta)\end{bmatrix} \quad (18)$$

$$0.2764=0.4-0.4\cos\delta \quad (19)$$

where $\tilde{\psi}_{rq}$, $\tilde{\psi}_{rd}$ are harmonic rotor fluxes of *d-q* frame; and the symbols with "~" denote the alternating components. Equation (19) presents an analytical relationship between the harmonic magnitude and the space angle difference.

The harmonic rotor fluxes of the *d-q* frame lead to harmonic back-EMFs which can be given by

$$\begin{bmatrix}\tilde{E}_{rd}\\ \tilde{E}_{rq}\end{bmatrix}=0.5528\omega\psi_{m3}\begin{bmatrix}2\sin(4\theta+0.5\delta)+1.618\sin(2\theta-\delta)\\ -2\sin(4\theta+0.5\delta)+1.618\sin(2\theta-\delta)\end{bmatrix} \quad (20)$$

Where $\tilde{E}_{rd}$ and $\tilde{E}_{rq}$ are the harmonic back-EMFs that originate from the third harmonics winding coils.

Also, transforming the additional harmonic inductances into the *d-q* frame yields:

$$\begin{bmatrix}\tilde{L}_d\\ \tilde{L}_q\end{bmatrix}\approx\eta_3 L_\theta\begin{bmatrix}0.691\cos(2\theta-\delta)+(0.0712\eta_3-1.809)\cos(4\theta+0.5\delta)\\ 0.691\cos(2\theta-\delta)+(1.809-0.0712\eta_3)\cos(4\theta+0.5\delta)\end{bmatrix} \quad (21)$$

Where $\tilde{L}_d$, and $\tilde{L}_q$ are the harmonic inductances of *d-q* frame which are calculated up to the order of 4; and η_3 is the third harmonic winding factor which is 1/3 for a motor with concentrated windings [27, 28]. The harmonic mutual-inductances are even frequencies, however, their expressions are too complex to represent currently.

Then the armature voltages under the *d-q* frame can be reformulated as

$$\begin{aligned}&\begin{bmatrix}E_{Ld}\\ E_{Lq}\end{bmatrix}\\ &=\frac{d}{dt}\left(\begin{bmatrix}L_d+\tilde{L}_d & \tilde{L}_{dq}\\ \tilde{L}_{qd} & L_q+\tilde{L}_q\end{bmatrix}\begin{bmatrix}i_d\\ i_q\end{bmatrix}\right)-\omega\begin{bmatrix}0 & 1\\ -1 & 0\end{bmatrix}\begin{bmatrix}L_d+\tilde{L}_d & \tilde{L}_{dq}\\ \tilde{L}_{qd} & L_q+\tilde{L}_q\end{bmatrix}\begin{bmatrix}i_d\\ i_q\end{bmatrix}\\ &=p\left(\begin{bmatrix}L_d & 0\\ 0 & L_q\end{bmatrix}\begin{bmatrix}i_d\\ i_q\end{bmatrix}\right)-\omega\begin{bmatrix}0 & 1\\ -1 & 0\end{bmatrix}\begin{bmatrix}L_d & 0\\ 0 & L_q\end{bmatrix}\begin{bmatrix}i_d\\ i_q\end{bmatrix}+\begin{bmatrix}\tilde{E}_{Ld}\\ \tilde{E}_{Lq}\end{bmatrix}\end{aligned} \quad (22)$$

and

$$\begin{bmatrix}\tilde{E}_{Ld}\\ \tilde{E}_{Lq}\end{bmatrix}=\frac{d}{dt}\left(\begin{bmatrix}\tilde{L}_d & \tilde{L}_{dq}\\ \tilde{L}_{qd} & \tilde{L}_q\end{bmatrix}\begin{bmatrix}i_d\\ i_q\end{bmatrix}\right)-\omega\begin{bmatrix}0 & 1\\ -1 & 0\end{bmatrix}\begin{bmatrix}\tilde{L}_d & \tilde{L}_{dq}\\ \tilde{L}_{qd} & \tilde{L}_q\end{bmatrix}\begin{bmatrix}i_d\\ i_q\end{bmatrix} \quad (23)$$

In the above relationships, E_{Ld} and E_{Lq} are the armature voltages of the *d-q* frame; $\tilde{E}_{Ld}$, $\tilde{E}_{Lq}$ are the harmonic armature voltages of the *d-q* frame; and $\tilde{L}_{dq}$, $\tilde{L}_{qd}$ are the harmonic mutual-inductances of the *d-q* frame.

Modify (1) with (19) and (22), a more comprehensive model incorporating harmonic winding coils is given by

$$\begin{aligned}\begin{bmatrix}u_d\\ u_q\end{bmatrix}&=R_s\begin{bmatrix}i_d\\ i_q\end{bmatrix}+\frac{d}{dt}\left(\begin{bmatrix}L_d & 0\\ 0 & L_q\end{bmatrix}\begin{bmatrix}i_d\\ i_q\end{bmatrix}\right)-\omega\begin{bmatrix}0 & 1\\ -1 & 0\end{bmatrix}\begin{bmatrix}L_d & 0\\ 0 & L_q\end{bmatrix}\begin{bmatrix}i_d\\ i_q\end{bmatrix}\\ &+\omega\psi_{m1}\begin{bmatrix}0\\ 0.6+0.4\cos\delta\end{bmatrix}+\begin{bmatrix}\tilde{E}_{Ld}+\tilde{E}_{rd}\\ \tilde{E}_{Lq}+\tilde{E}_{rq}\end{bmatrix}\end{aligned} \quad (24)$$

Providing the faulty motor is operated under the constant u_d and u_q, then the harmonic currents can be given by

$$\begin{bmatrix}\tilde{i}_d\\ \tilde{i}_q\end{bmatrix}=-\begin{bmatrix}R_s+sL_d & -\omega L_q\\ \omega L_d & R_s+sL_q\end{bmatrix}^{-1}\begin{bmatrix}\tilde{E}_{Ld}+\tilde{E}_{rd}\\ \tilde{E}_{Lq}+\tilde{E}_{rq}\end{bmatrix} \quad (25)$$

Where $\tilde{i}_d$, and $\tilde{i}_q$ are the harmonic currents under the *d-q* frame; and *s* refers to the Laplace operator.

As revealed by (25), most current harmonics are produced as the result of the third harmonics of back-EMFs and armature voltages. Therefore, it is stressed here that the existing current harmonics are more related to the stator winding distribution manner.

IV. Feasible PWM Techniques

A. Q-SPWM (Quasi-SPWM)

Assume the *x-y* frame references are known now, then the demanded pole voltages to drive this quasi 3Ph motor can be straightforwardly derived by the inverse transformation of (16), and the result is shown as below.

$$\begin{bmatrix} u_{CO} & u_{DO} & u_{EO} \end{bmatrix}^{\mathrm{T}} = \begin{bmatrix} \mathbf{T}_{Ploe2xy} \end{bmatrix}^{-1} \begin{bmatrix} v_x & v_y & v_{o,ref} \end{bmatrix}^{\mathrm{T}}, v_{o,ref} \equiv 0 \quad (26)$$

where u_{CO}, u_{DO}, u_{EO} from now on denote the modulation signals of this Q-SPWM, and this PWM technique is currently the most simple and effective. As the name suggests, the modulation signals of this Q-SPWM are not purely sinusoidal out of some back-EMF injection. Notice that this Q-SPWM neither belongs to the CBPWM category which is featured by a zero-sequence signal injection.

In most articles targeting at a balanced system [20, 22, 23], the modulation index is defined as:

$$M = \frac{V^*}{0.5U_{dc}} \quad (27)$$

where M is the general modulation index and V^* is the peak value of the fundamental phase voltage references. V^* equals the amplitude of *d-q* frame reference voltages in a balanced system. However, three coordinate frames exist regarding this unbalanced system, *i.e.*, *d-q* frame, and α-β frame, and *x-y* frame, and worse still, the reference voltage vector length varies from one coordinate frame to another. In this context, the modulation index of this unbalanced system is defined as:

$$M = \frac{max\left(u_{CN}, u_{DN}, u_{EN}\right)}{0.5U_{dc}} \quad (28)$$

Then, the DC bus utilization is defined as the ratio of the magnitude of *d-q* frame reference voltages to one-half U_{dc} when M is unity. This definition is consistent with the understanding of the DC bus utilization in a balanced system.

$$DC_{usage} = \frac{\sqrt{u_d^2 + u_q^2}\big|_{@M=1}}{0.5U_{dc}} \quad (29)$$

On the other hand, the peak values of pole voltage references are not allowed to exceed one-half U_{dc}, otherwise, overmodulation will occur. Given this fact, another modulation index, pole voltage modulation ratio, is defined as:

$$M_{pole} = \frac{max\left(u_{CO}, u_{DO}, u_{EO}\right)}{0.5U_{dc}} \quad (30)$$

where M_{pole} denotes the modulation ration of pole voltages and is dependent on the motor speed providing ψ_{m1} and ψ_{m3} are known to the control system. Thus, PWM performance can be justified by examining the above two factors.

B. SVPWM

TABLE I
Basic space vectors in the case of adjacent phase open fault

The SV coding ($[S_C,S_D,S_E]$)	Angle and length of basic space vectors
V_0(000)	0∠0°
V_1(001)	$0.3914U_{dc}$∠-40.3885°
V_2(010)	$0.1843U_{dc}$ ∠-144.0069°
V_3(011)	$0.3914U_{dc}$∠-67.6087°
V_4(100)	$0.3914U_{dc}$∠112.3913°
V_5(101)	$0.1843U_{dc}$∠35.9931°
V_6(110)	$0.3914U_{dc}$∠139.6115°
V_7(111)	0∠0°

The drifting neutral effect can be alleviated with the proposed affine transformation in (17), and therefore one only needs to concentrate on the voltage vector synthesis with the eight basic space vectors (SVs) of the *x-y* plane. The eight basic space vectors of the *x-y* plane are presented in TABLE I with a graphical representation in Fig.4.

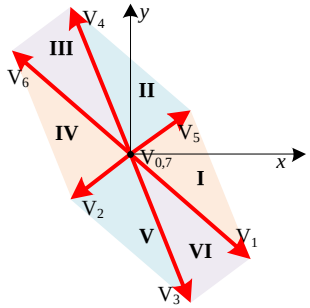

Fig. 4 The basic SVs under adjacent-phase open fault become unevenly distributed on the presented *x-y* plane

From Fig.4, the six non-zero vectors (V_1-V_6) shape an irregular hexagon outline, with two zero-vectors in the origin of this hexagon. The angle interval between two adjacent SVs is not 60° any longer, and this phenomenon is a little different from a balanced 3Ph system. The basic SVs are grouped into three parts, *i.e.*, four large vectors with a length of $0.3914U_{dc}$, two small vectors with a length of $0.1843U_{dc}$, and two zero-vectors. Accordingly, the *x-y* plane is divided into six sectors as revealed by Fig.4. Within each sector, the reference voltage vector can be synthesized by the adjacent SVs.

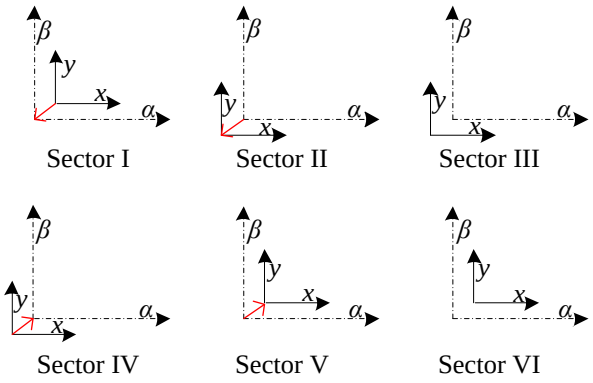

Fig.5 The location of the kinetic *x-y* frame relative to the stationary α-β frame at each sector.

Fig.5 shows the position of the *x-y* frame relative to the stationary α-β frame. From Fig.5, the relative location between these two frames is constantly changing during one fundamental cycle. For instance, in sector I, the *x-y* frame moves towards the origin of the α-β frame as the voltage reference vector starts from V_1 and traverses sector I. The red arrow denotes the movement path and direction. Notice that no arrow is marked in sectors III and VI, however, this does not mean there is no relative movement. In fact, the movement path in these sectors is just too short to mark. Since the basic SVs under the *x-y* frame are time-invariant, the reference voltage vector, which is also mapped onto the *x-y* plane with the affine transformation, can be conveniently synthesized under the kinetic *x-y* frame.

The calculation procedure of the presented SVPWM is the same as the one for conventional 3Ph drives, except for the sector identification. Nevertheless, the sector number can be univocally identified by coordinating the sign of three trigonometric functions as shown in Table II.

TABLE II
SVPWM Sector identification

Sector No.	$\lvert \mathbf{V_{ref}} \rvert \sin(\lambda\text{-}35.9931^{o})$	$\lvert \mathbf{V_{ref}} \rvert \sin(\lambda\text{-}112.3913^{o})$	$\lvert \mathbf{V_{ref}} \rvert \sin(\lambda\text{-}139.6115^{o})$
I	≤0	≤0	≤0
II	>0	≤0	≤0
III	>0	>0	≤0
IV	>0	>0	>0
V	≤0	>0	>0
VI	≤0	≤0	>0

In Table II, the angle λ stands for the position of $\mathbf{V_{ref}}$ of the *x-y* frame. The trigonometric function, for instance, $\sin(\lambda\text{-}35.9931^{o})$, can be inferred by

$$|\mathbf{V_{ref}}|\sin\left(\lambda-35.9931^{o}\right)=\left(v_x\cos 35.9931^{o}-v_y\sin 35.9931^{o}\right) \quad (31)$$

Fig.6 summarizes the switching pattern for the presented SVPWM under a two-phase open circuit. From Fig.6, the reference voltage synthesis for a 5Ph inverter under two-phase open-circuit can be likewise arranged in a symmetrical and center-aligned pattern to limit the switching losses. The adopted switching pattern is of classical seven-segment design, starting and ending with the same zero vector, and it ensures that only one switch status changes at each instant.

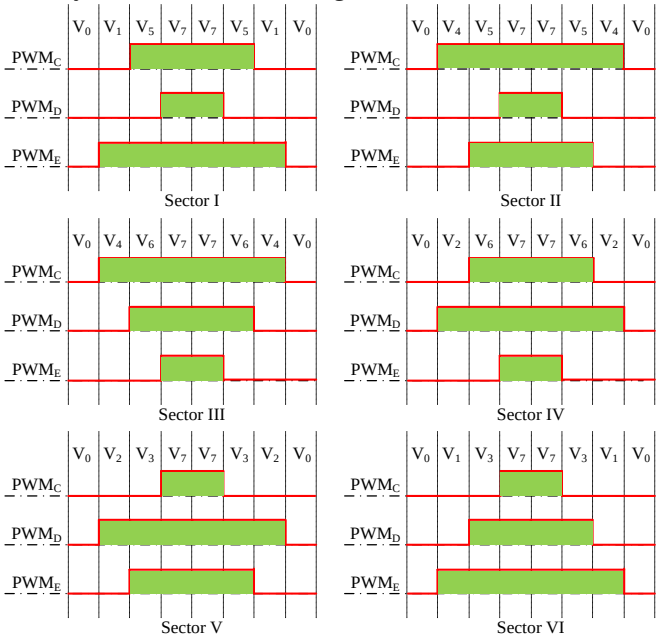

Fig.6 The center-aligned seven-segment switching pattern in each sector to lower switching losses

C. *Min-max CBPWM* (*An easy SVPWM*)

The SVPWM is criticized by its complexities and to this end, a min-max CBPWM is suggested in some articles, which has been justified as identical to the SVPWM. This CBPWM can be independent of the phase number and modulation signal shapes [20, 22, 23], and it is, therefore, very likely to be applicable to this unbalanced drive. In the min-max CBPWM, a common-mode signal (CMS) is first extracted from the pole voltage references, and it is later assigned to $v_{o,ref}$ in Fig.3.

In the case of two-phase open faults, this CMS is given by:

$$u_{cms}=0.5\left(u_{max}+u_{min}\right) \quad (32)$$

$$\begin{cases} u_{max}=max\left(u_{CO},u_{DO},u_{EO}\right) \\ u_{min}=min\left(u_{CO},u_{DO},u_{EO}\right) \end{cases} \quad (33)$$

where u_{max}, and u_{min} denote, respectively, the maximum and minimum values of pole voltage references; and u_{cms} is the collected common-mode signal which is of 3rd harmonic.

Then, this CBPWM approach injects a zero-sequence signal by the following manipulation

$$\begin{bmatrix} v_{CO} & v_{DO} & v_{EO} \end{bmatrix}^{\mathrm{T}}=\left[\mathbf{T}_{Ploe2xy}\right]^{-1}\begin{bmatrix} v_x & v_y & v_{o,ref} \end{bmatrix}^{\mathrm{T}},\ v_{o,ref}=-u_{cms} \quad (34)$$

where v_{CO}, v_{DO}, v_{EO} stand for the modulation signals of this min-max CBPWM which offers the same performance as the SVPWM. Thus, in this paper, the min-max CBPWM is also termed "an easy SVPWM". The min-max CBPWM is not an innovation of this work, however, this work is the first attempt on a 5Ph drive with two-phase open-circuited. Notice that in the experiments, this easy SVPWM is merged with the SVPWM since they have the same performance.

As a demonstration, Fig.7 evolves the experimental procedure to implement the CMS injection-based CBPWM. First, extract the CMS from u_{CO}, u_{DO}, u_{EO} as illustrated in Fig.7(a); then subtract u_{CMS} from u_{CO} and it yields the modulation signal v_{CO} as shown in Fig.7(b); and repeat Fig.7(b) by replacing u_{CO} with, respectively, u_{DO} and u_{EO}, one can have all modulation signals as shown in Fig.7(c).

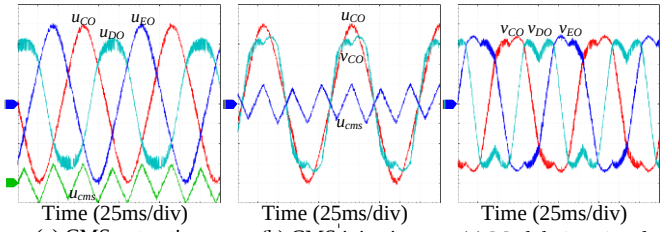

Fig.7 Experimental procedures to implement the min-max CBPWM. The vertical axis is scaled to 12V/div.

V. Non-adjacent-phase Open Fault

A. *The proposed affine transformation*

Suppose phase-A and -C are open-circuited, then the drifting neutral effect can be mathematically represented by (35). The formula deduction can reference the case of the adjacent phase open fault and, thus, it is not elaborated here.

$$\begin{bmatrix} u_\alpha \\ u_\beta \\ u_o \end{bmatrix}=\left[\mathbf{T}_{ploe2xy}\right]\begin{bmatrix} u_{BO} \\ u_{DO} \\ u_{EO} \end{bmatrix} + \frac{2\left(u_{AN}+u_{CN}\right)}{5}\begin{bmatrix} \cos 2\delta+\dfrac{1+\cos 2\delta}{3} \\ \tan\delta\cos 2\delta+\dfrac{\sin 2\delta}{3} \\ 0 \end{bmatrix}+\begin{bmatrix} 0 \\ 0 \\ -\dfrac{6}{5}u_{NO} \end{bmatrix} \quad (35)$$

where $[T_{pole2xy}]$ is used to signify that the pole voltage references in this fault case also require re-mapping to offset the drifting neutral effect.

This $[T_{pole2xy}]$ is given by

$$\left[\mathbf{T}_{ploe2xy}\right]=\frac{2}{5}\begin{bmatrix}\cos\delta+\frac{1+\cos 2\delta}{3} & \cos 3\delta+\frac{1+\cos 2\delta}{3} & \cos 4\delta+\frac{1+\cos 2\delta}{3}\\ \sin\delta+\frac{\sin 2\delta}{3} & \sin 3\delta+\frac{\sin 2\delta}{3} & \sin 4\delta+\frac{\sin 2\delta}{3}\\ 1 & 1 & 1\end{bmatrix} \tag{36}$$

Thus, the affine transformation, in this case, is given by

$$\begin{bmatrix}v_x\\ v_y\\ v_o\end{bmatrix}=\begin{bmatrix}1 & 0 & 0.2981 & 0\\ 0 & 1 & 0.9176 & 0\\ 0 & 0 & 0 & 1\end{bmatrix}\begin{bmatrix}u_\alpha\\ u_\beta\\ e_A+e_C\\ u_o+\frac{6}{5}u_{NO}\end{bmatrix} \tag{37}$$

B. PWM techniques

In common with the adjacent-phase open fault, there are three PWM techniques available in this fault case, and they involve a similar design procedure and, thus, are not detailed here. The eight basic space vectors are summarized in Table III and graphically depicted in Fig.8. The SVPWM under this fault type is similar to the adjacent-phase open fault and can be replaced by an analogous CBPWM as illustrated in (32)~(34).

TABLE III
Basic space vectors in the case of non-adjacent-phase open fault

The SV coding ($[S_B,S_D,S_E]$)	Angle and length of the SVs
V_0(000)	0∠0°
V_1(001)	$0.3369U_{dc}$∠-63.7316°
V_2(010)	$0.3369U_{dc}$∠-152.2708°
V_3(011)	$0.4824U_{dc}$∠-108.003°
V_4(100)	$0.4824U_{dc}$∠71.997°
V_5(101)	$0.3369U_{dc}$∠27.7292°
V_6(110)	$0.3369U_{dc}$∠116.2684°
V_7(111)	0∠0°

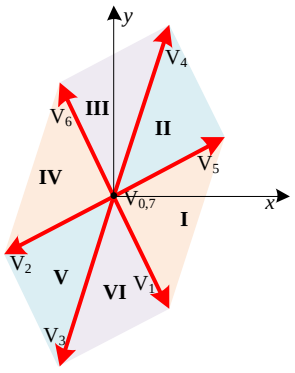

Fig. 8 The basic SVs under non-adjacent-phase open fault

VI. Experimental Results

Fig.9 demonstrates the test rig of a laboratory-scale 5Ph drive, which comprises a 5Ph half-bridge inverter and a generic 5Ph PMSM mechanically coupled with a DC generator, to evaluate the performance of the involved PWM approaches. A 32-bit floating-point DSP (TMS320F28335, and the FPGA in Fig.9 is bypassed) is chosen to implement the overall control algorithms. The rotational inertia of this drive is 0.12kg·m^2, the DC Bus voltage is fixed to about 240V, the switching frequency is 10kHz, and the parameters of 5Ph PMSM are shown in Table IV. The open-loop control with a zero u_d and a constant u_q is adopted to spin the motor.

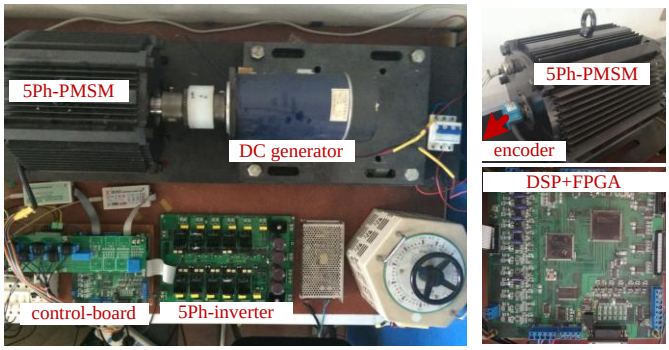

Fig.9 Laboratory-scale experimental setup

TABLE IV
Parameters of the studied trapezoidal back-EMF 5Ph PMSM

Symbol	Description	Value
ψ_{m1}	First harmonic rotor flux	0.535872 Wb
ψ_{m3}	Third harmonic rotor flux	0.033492 Wb
R	Resistance	1.1 Ω
P	Pole pairs	2
L_d	d-inductance of 1st subspace	6.54 mH
L_q	q-inductance of 1st subspace	8.32 mH
L_{d3}	d-inductance of 3rd subspace	1.34 mH
L_{q3}	d-inductance of 3rd subspace	2.06 mH

A. Phase-A and -B open fault test

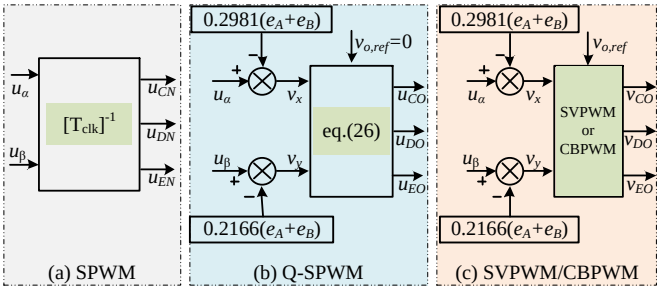

Fig.10 Several PWM techniques for the faulty motor drive. (a) the SPWM for most balanced systems; (b) the Q-SPWM for this unbalanced system; and (c) the min-max CBPWM and/or SVPWM for this unbalanced system.

Fig.10 shows several PWM techniques that seem applicable to the system studied. In the SPWM, the sinusoidal outputs of the inverse Clarke transformation are used as the modulation signals, and this technique is widely accepted in balanced systems. In Fig.10(a), the modulation signals are represented by u_{CN}, u_{DN}, u_{EN} since the phase voltages are deemed identical to the pole voltages in a balanced system. In the Q-SPWM, the drifting neutral effect has been incorporated into the control scheme, and the modulation signals are represented by u_{CO}, u_{DO}, u_{EO}. Finally, both SVPWM and the min-max CBPWM have been widely accepted to be interchangeable, thus they are merged into one scheme where the modulation signals are represented by v_{CO}, v_{DO}, v_{EO}.

Fig.11 shows voltage vector reference remapping from the α-β plane to the x-y plane. The voltages u_α and u_β are obtained by the inverse park transformation of u_d and u_q, and they form

a circularly rotating voltage vector on the α-β plane for the FOC purpose. Undoubtedly, it leads to a false phase voltage when directly applying u_α and u_β to this unbalanced drive. The drifting neutral appears when the motor starts spinning and its impact can be weakened by incorporating the failed phase back-EMFs while implementing the PWM as shown in Fig.11(b).

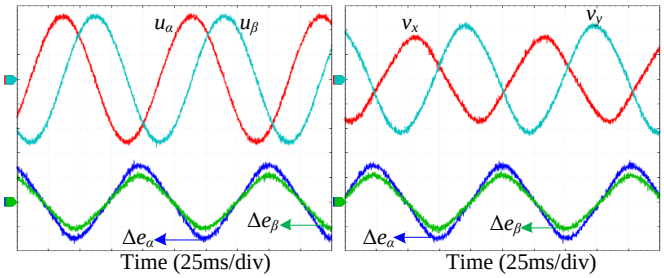

(a) Original reference voltages and Δe_α and Δe_β (b) Reference voltages after remapping with Δe_α and Δe_β

Fig.11 The reference voltage remapping with the back-EMF information of open phases. All voltages are scaled to 12.5V/div, with Δe_α=-0.2981(e_A+e_B) and Δe_β=-0.2166(e_A+e_B).

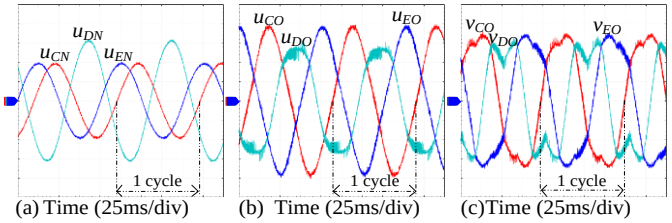

(a) Time (25ms/div) (b) Time (25ms/div) (c)Time (25ms/div)

Fig.12 Modulation waveforms under (a) SPWM; b) Q-SPWM; and c) SVPWM and/or CBPWM. The voltages in (a) are scaled to 24V/div, and in (b) and (c) are scaled to 12V/div.

Fig.12 reveals, respectively, the modulation waveforms of SPWM, Q-SPWM as well as SVPWM and/or CBPWM. In this test, the motor is operated to 300 rpm with a constant u_q of 21.5V in the SPWM case and 32V in both Q-SPWM and SVPWM/CBPWM cases. In the SPWM case, the modulation signals can be magnified by the Clarke matrix of (4) which is not the unitary transformation. This test explains why the demanded u_q in SPWM case is lower than the ones in both Q-SPWM and SVPWM/CBPWM cases that further utilize the back-EMF information to reshape their modulation signals. This result suggests that the DC bus utilization under SPWM is quite low.

In Figs.12(b) and (c), the modulation waveforms are properly rectified by incorporating the failed phase back EMFs to offset the drifting neutral effect. From Figs.12(b) and (c), the demanded pole voltages under SVPWM/CBPWM are, respectively, 42.1V, 35.9V, and 42.1V; whereas these values are, respectively, 47.6V, 31.5V, and 47.6V under the Q-SPWM. This result means that under Q-SPWM the demanded pole voltages to spin the motor at a certain speed are, respectively, 1.13, 0.88, and 1.13 times those of SVPWM/CBPWM case. It should be noted that the calculation of DC bus utilization should reference phase-C and/or phase-E which are more likely to be overmodulated. Under this speed, the DC bus utilization of SVPWM/CBPWM is 13% higher than that of Q-SPWM. It is important to notice that in the fault mode the DC bus utilization varies, depending on the motor speeds, and accordingly, some plots indicating the pole voltage modulation ratio and DC bus utilization can be drawn and are illustrated in Fig. 13.

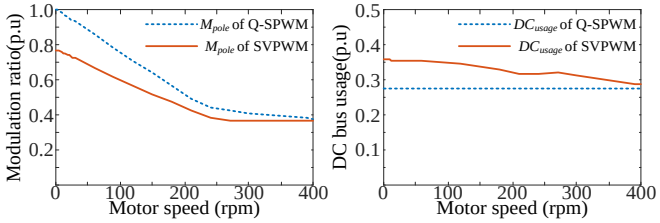

(a) Modulation ratio over speed (b) DC bus suage over speed

Fig.13 Modulation ratio and DC bus utilization over speed under, respectively, Q-SPWM and SVPWM/CBPWM, in the case of adjacent phase open fault.

Fig.13 reveals the pole voltage modulation ratio and DC bus utilization of, respectively, the Q-SPWM and SVPWM/CBPWM. The drifting neutral is negligible at around zero speed, and in this case, the pole voltage can be deemed equal to the phase voltage. As the speed increases, the drifting neutral is getting more severe, and to cope with this problem, the demanded voltage has to be redefined according to the estimated drifting neutral, which leads to a declined M_{ploe} as revealed by Fig.13(a). Because of the injection of a common mode signal, M_{ploe} of SVPWM/CBPWM is smaller than the one of Q-SPWM as shown in Fig.13(a). From Fig.13 (b), the measured DC_{usage} of the Q-SPWM is merely 0.276 which signifies a serious derating. From Fig.13(b), DC_{usage} of the SVPWM/CBPWM can be increased up to 0.357 at a standstill, and it starts to drop as the motor speed increases and is still 4% higher at 400 rpm (beyond this speed is the overmodulation region). As a conclusion, the SVPWM outperforms the Q-SPWM in terms of DC bus utilization.

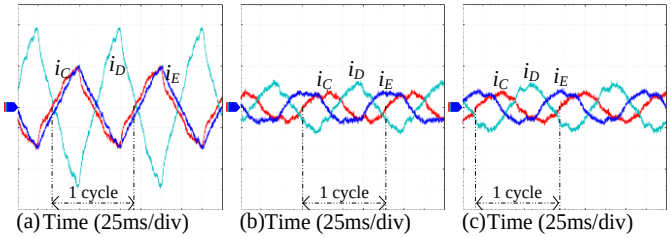

(a)Time (25ms/div) (b)Time (25ms/div) (c)Time (25ms/div)

Fig.14 Phase currents under (a) SPWM; b) Q-SPWM; and c) SVPWM/CBPWM. The phase currents are scaled to 10A/div.

Fig.14 shows phase currents under SPWM, Q-SPWM, and SVPWM/CBPWM, respectively. From Fig.14(a), phase currents are seriously distorted by the harmonics, and they are more intuitive under the α-β frame. This result implies that under SPWM the motor currents are not dictated to the d-q frame voltage commands out of the drifting neutral. From Figs.14(b) and (c), the α-β frame currents are much more sinusoidal, and the existing low-order current harmonics are explained by the third harmonic winding coils.

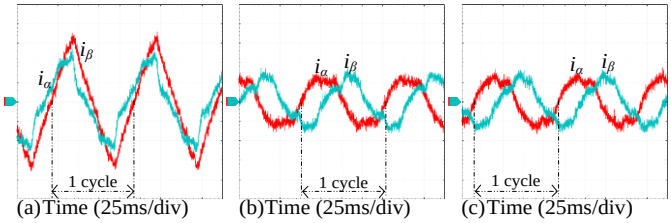

(a)Time (25ms/div) (b)Time (25ms/div) (c)Time (25ms/div)

Fig.15 Currents of the α-β frame under (a) SPWM; b) Q-SPWM; and c) SVPWM/CBPWM. The currents are scaled to 5A/div.

Fig.15 shows the α-β frame currents under SPWM, Q-

SPWM, and SVPWM/CBPWM, respectively. In this experiment, the currents are transformed into the α-β frame with the inverse Clarke matrix. One can notice that i_α and i_β are almost overlapped under SPWM. In contrast, the currents under SVPWM and CBPWM are more desirable for being orthogonal to each other, and this result also indicates the fundamental MMF is more controllable under Q-SPWM as well as SVPWM and CBPWM.

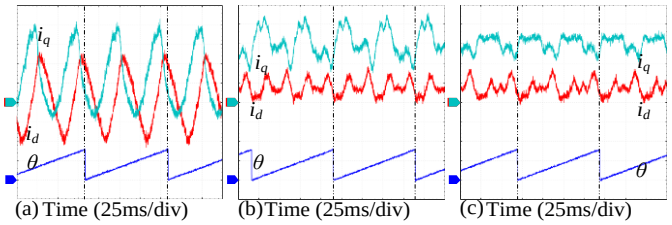

Fig.16 Currents of *d-q* frame under (a) SPWM; b) Q-SPWM; and c) SVPWM/CBPWM. The position is scaled to 240 deg/div; and currents in (a) are scaled to 5A/div, in (b) as well as (c) scaled to 1A/div.

Fig.16 shows *d-q* frame currents under SPWM, Q-SPWM, and SVPWM/CBPWM, respectively. During the test, the drive is loaded via the shaft coupled DC generator with a resisting torque of 8.2 Nm. From Fig.16(a), the *d-q* frame currents oscillate significantly, and this is caused by the ill-considered drifting neutral in the SPWM case. The drifting neutral effect is alleviated under both Q-SPWM and SVPWM/CBPWM techniques. Theoretically, the *d-q* frame current fluctuation can be fully removed regarding a sinusoidal back-EMF PMSM. However, for this trapezoidal back-EMF motor (a more universal motor type), the *d-q* frame rotor fluxes and inductances are not that flat and this fact leads to some low-order harmonic currents. The harmonic currents of the *d-q* frame further result in certain torque oscillation, however, from Fig.16(a) it is hard to observe the position oscillation because of the large rotational inertia of the motor drive.

The FFT (Fast Fourier Transform) is an important tool to examine the current harmonics. However, in this unbalanced system, the expected orthogonality of i_α and i_β can be missing as evident in the SPWM case. To this end, THD is performed on *d-q* frame currents since only the wanted components of i_α and i_β are translated to 0Hz with all the others being AC signals. Thus, the FFT on *d-q* frame currents is more rational to evaluate the MMF under different PWM techniques.

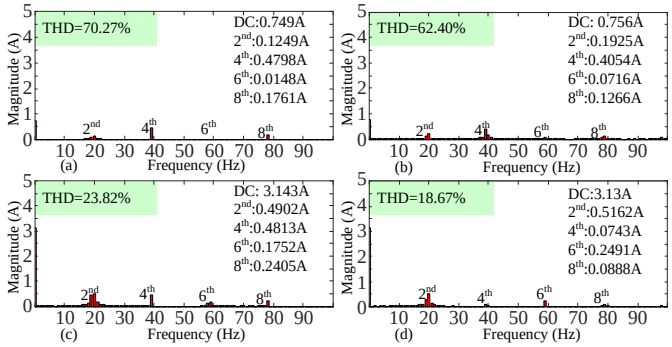

Fig.17 Harmonic contents of: (a) i_d under Q-SPWM, (b) i_d under SVPWM/CBPWM, (c) i_q under Q-SPWM, and (d) i_q under SVPWM/CBPWM.

Fig.17 reveals the harmonic current contents of the *d-q* frame under, respectively, Q-SPWM and SVPWM/CBPWM. The FFT is able to measure each harmonic without knowing the fundamental frequency. Herein, the duration time window for FFT is 100ms. Consequently, the THD of i_d is 70.27% under Q-SPWM and 62.4% under SVPWM/CBPWM; whereas the THD of i_q is 23.82% under Q-SPWM and 18.67% under SVPWM/CBPWM. Generally, the THD of i_d is relatively larger than the one of i_q, and the reason is that i_d is almost null such that the harmonics are dominant. The existing harmonic currents are caused by the harmonic rotor fluxes and harmonic inductances that are unable to get decoupled under the *d-q* frame (refer to (20) and (21)). As a conclusion, the advantage of SVPWM/CBPWM is marginal in terms of the current distortion.

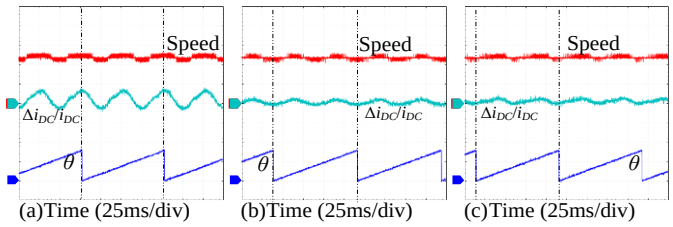

Fig.18 Torque behavior under (a) SPWM; b) Q-PWM; and c) SVPWM/CBPWM. The speed is scaled to 120 rpm/div; $\Delta i_{DC}/i_{DC}$ scaled to 0.1/div; position scaled to 240 deg/div.

Fig.18 refers to the torque behavior of this faulty motor under SPWM, Q-SPWM, and SVPWM/CBPWM, respectively. Since we have no torque transducer to capture the high dynamic electromagnetic torque, it is sensible to use the output current of the DC generator (i_{DC}) as an indication of the electromagnetic torque. From this figure, the torque-ripple is considerable under SPWM, however, it decreases remarkably under Q-SPWM and SVPWM/CBPWM. The torque-ripple intensity under SVPWM/CBPWM is almost identical to the one under Q-SPWM. However, it must be noted that the presented method is only intended for the correct modulation of fundamental phase voltages, and it plays a limited role in the reduction of harmonic torques. The torque ripple reduction can be achieved with a higher-level FTC, however, this exploration is beyond the scope of this paper.

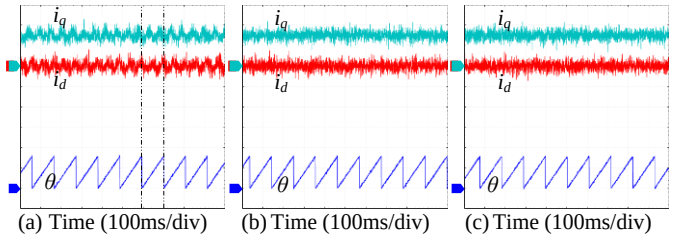

Fig.19 Current closed-loop performance using PIRs: (a) under the SPWM in the previous article, (b) under the presented Q-SPWM, and (c) under the presented SVPWM/CBPWM. The currents are scaled to 2A/div, position scaled to 240 deg/div.

Fig.19 demonstrates the current closed-loop performance using PIRs under, respectively, the SPWM in the previous article as well as the presented Q-SPWM and SVPWM/CBPWM. In the test, the faulty motor operates in a constant torque mode with i_q=3A. This test attempts to eliminate the (existing) harmonic currents using PIRs whose preferences are maintained the same in these three cases. From Fig.19, the harmonic currents are generally attenuated under PIRs. But when observing Fig.19(a), the harmonic currents are

not eliminated completely. Some researchers might argue that the parameters of PIR in Fig.19(a) may not be optimal, however, this is not the case. The motor speed varies more severely under SPWM such that the PIRs' bandwidth in Fig.19(a) is wider by degrading the steady-state tracking performance. The bandwidth of PIRs in Fig.19(b) and (c) also references the SPWM case, yet they show a better tracking performance. This test confirms that the fundamental MMF is more controllable under the proposed affine transformation.

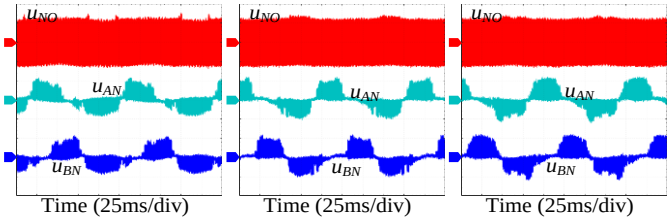

Fig.20 The voltages of neutral point and open phases under (a) SPWM; b) Q-PWM; and c) SVPWM/CBPWM. The voltages are scaled to 100V/div.

Fig.20 refers to the voltages of the neutral point and open-circuited phases under different PWM techniques. Unfortunately, it is difficult to directly observe the oscillatory neutral effect which is lost in the ambient switching noises. This phenomenon is normal since, as per (9), u_{NO} comprises considerable switching voltages (common-mode voltages in many articles), other than u_{AN} and u_{BN}. Besides, from Fig.20, the open phase voltages, u_{AN} and u_{BN}, are also choppy, and the switching noises originate from the mutually induced EMFs. From Fig.20, u_{AN} and u_{BN} in the three sub-figures are almost identical in magnitude since they are only determined by the speed. Overall, this test demonstrates that drifting neutral is related to the motor speed and is impossible to be canceled physically.

B. Phase-A and -C open fault test

The SPWM has been proven unsuitable for an unbalanced drive and thus, only the Q-SPWM and SVPWM/CBPWM are investigated and compared in this section.

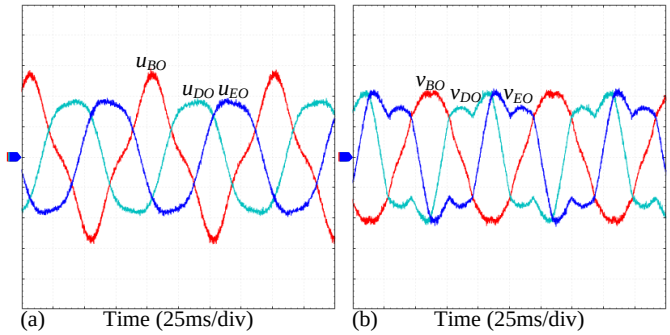

Fig.21 In the case of a non-adjacent-phase open fault, the modulation waveforms of (a) Q-SPWM; and b) SVPWM/CBPWM. The vertical axis is scaled to 25V/div.

Fig.21 shows the modulation waveforms of Q-SPWM and SVPWM/CBPWM, respectively. During this test, u_q is adjusted to 16V to operate the motor at 300 rpm. The demanded u_q, in this case, is much lower than the one under the adjacent-phase open fault, and the reasons for this can be explained by its decoupled model which has a lower *d-q* frame rotor flux (refer to [17]). The demanded pole voltages under the Q-SPWM are, respectively, 65V, 40V, and 40V; and they are all 50V under the SVPWM/CBPWM. Evidently, the DC bus utilization of SVPWM/CBPWM is 30% higher than that of Q-SPWM under the current speed.

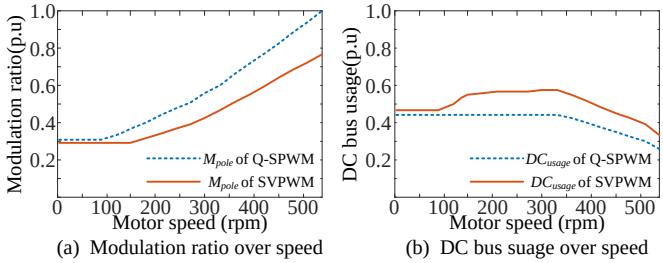

Fig.22 In the case of a non-adjacent-phase open fault, the pole voltages modulation ratio and DC bus utilization over speed under, respectively, Q-SPWM and SVPWM/CBPWM.

Fig.22 reveals the DC bus utilization and pole voltage modulation ratio of Q-SPWM and SVPWM/CBPWM under non-adjacent-phase open fault. In this fault case, it is possible to operate the motor at up to 540 rpm (beyond this speed is the overmodulation region). From Fig.22(a), Both curves increase with the motor speed, and as expected, the M_{ploe} of SVPWM/CBPWM is always to be smaller. Under Q-SPWM, the DC bus utilization ranges between 0.535 and 0.276. In contrast, the DC bus utilization of SVPWM/CBPWM is within 0.695 and 0.359, and it could be 30% higher than the Q-SPWM at 300 rpm and the above. Once again, it confirms that the SVPWM/CBPWM outperforms the Q-SPWM in terms of DC bus utilization.

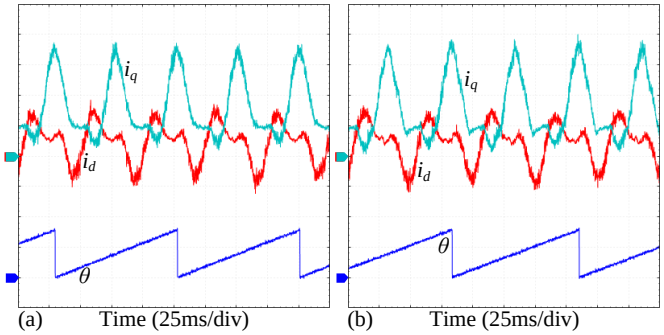

Fig.23 In the case of a non-adjacent-phase open fault, the *d-q* frame current waveforms under a) Q-SPWM; and b) SVPWM/CBPWM. The currents are scaled to 2 A/div.

Fig.23 shows *d-q* frame currents under, respectively, Q-SPWM and SVPWM/CBPWM. From this figure, the *d-q* frame currents are likewise ripply even after the affine transformation. These ripples also result from the third harmonic winding coils which are manifested as alternating EMFs under the *d-q* frame. Additionally, the ripples of *d-q* frame currents are more significant than the ones under adjacent-phase open fault, and this phenomenon can be explained by the third harmonics rotor fluxes which are more significant in this fault case (refer to (18), (21), (A6), (A8)).

Fig.24 summarises the current THDs under non-adjacent-phase open fault at about 300 rpm. In this fault case, the THD under SVPWM/CBPW is somehow larger than the one under Q-SPWM. It is worth recalling that a 5Ph PMSM is more complex than expected, and it is, therefore, difficult to establish a comprehensive analytic model that incorporates all the system uncertainties to predict the harmonic currents.

However, it is safe to conclude that harmonics are mainly caused by the third harmonic winding coils. Nevertheless, the enhanced control of the fundamental MMF has been successful.

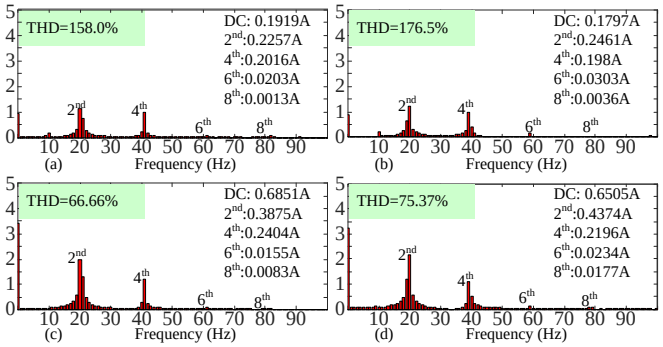

Fig.24 In the case of non-adjacent-phase open fault, the harmonic contents of: (a) i_d under Q-SPWM, (b) i_d under SVPWM/CBPWM, (c) i_q under Q-SPWM, and (d) i_q under SVPWM/CBPWM.

C. A brief summary

In this section, it is experimentally proved that the classical SPWM typically for a balanced system is not suitable any longer, and the presented Q-SWPM and SVPWM/CBPWM can be a replacement for 5Ph PMSMs with two-phase open-circuited. Generally, both SVPWM and CBPWM are superior to Q-SPWM in DC bus utilization and overall switching losses. In terms of current harmonics, the advantages of SVPWM and CBPWM are marginal and even controversial considering different fault types. The main demerit of SVPWM concerns complex implementation, and in this regard, the SVPWM can be replaced by the min-max CBPWM.

VII. Conclusions

In this paper, the neutral drifting issue of a generic 5Ph PMSM under two-phase open faults is addressed, which accounts for the failure of the classical SPWM. A kinetic reference frame is put forward which rectifies the SPWM and enhances the controllability of the fundamental MMF. Several PWM approaches are attempted, and the validity of the proposed nonlinear transformation to offset the drifting neutral effect is proved both theoretically and experimentally. Besides, the experimental results confirm that SVPWM and CBPWM outperform the Q-SPWM in terms of DC bus utilization and switching losses. On the other hand, CBPWM is more advantageous than SVPWM for having an identical output performance but a lower computational burden. Regarding the investigated motor type, there exist some harmonic currents that originate from third harmonic winding coils, and given this problem, some closed-loop harmonic elimination techniques are still necessary. Finally, it is worth emphasizing that the drifting neutral is not and can never be eliminated physically, however its impacts on PWM implementation can be canceled by properly redefining the pole voltage references, and this discovery is the major contribution of this work.

VIII. Appendix

A. Proof of the equation (8)

The 5Ph PMSM under undamaged state can be modeled as[27, 28]

$$\begin{bmatrix} u_{AN} \\ u_{BN} \\ u_{CN} \\ u_{DN} \\ u_{EN} \end{bmatrix} = R_s \begin{bmatrix} i_A \\ i_B \\ i_C \\ i_D \\ i_E \end{bmatrix} + \frac{d}{dt}\left(\begin{bmatrix} L_{AA} & L_{AB} & L_{AC} & L_{AD} & L_{AE} \\ L_{BA} & L_{BB} & L_{BC} & L_{BD} & L_{BE} \\ L_{CA} & L_{CB} & L_{CC} & L_{CD} & L_{CE} \\ L_{DA} & L_{DB} & L_{DC} & L_{DD} & L_{DE} \\ L_{EA} & L_{EB} & L_{EC} & L_{ED} & L_{EE} \end{bmatrix} \begin{bmatrix} i_A \\ i_B \\ i_C \\ i_D \\ i_E \end{bmatrix} \right) + \begin{bmatrix} e_A \\ e_B \\ e_C \\ e_D \\ e_E \end{bmatrix} \tag{A1}$$

where L_{ij}, with i and j=A,B,C,D,E, is the self- or mutual-inductance. The analytic model of phase inductances is very complex, nevertheless, one can always have the followings:

$$\begin{cases} L_{AA}+L_{BA}+L_{CA}+L_{DA}+L_{EA} \equiv \text{constant} \\ L_{AB}+L_{BB}+L_{CB}+L_{DB}+L_{EB} \equiv \text{constant} \\ L_{AC}+L_{BC}+L_{CC}+L_{DC}+L_{EC} \equiv \text{constant} \\ L_{AD}+L_{BD}+L_{CD}+L_{DD}+L_{ED} \equiv \text{constant} \\ L_{AE}+L_{BE}+L_{CE}+L_{DE}+L_{EE} \equiv \text{constant} \end{cases} \tag{A2}$$

$$e_A+e_B+e_C+e_D+e_E \equiv 0 \tag{A3}$$

$$i_A+i_B+i_C+i_D+i_E \equiv 0 \tag{A4}$$

The sum of the five phase voltages yields

$$u_{AN}+u_{BN}+u_{CN}+u_{DN}+u_{EN}=0 \tag{A5}$$

B. harmonic rotor fluxes and harmonic inductances (under phase-A and -C open fault)

Under the Clarke and Park transformations for the case of a non-adjacent-phase open fault, the 3rd harmonic rotor fluxes of the energized windings can be represented by:

$$\begin{bmatrix} \tilde{\psi}_{rd} \\ \tilde{\psi}_{rq} \end{bmatrix} = 0.7236\psi_{m3} \begin{bmatrix} \cos(4\theta+\delta)-1.618\cos(2\theta+0.5\delta) \\ \cos(4\theta+\delta)+1.618\cos(2\theta+0.5\delta) \end{bmatrix} \tag{A6}$$

$$0.7236 = 0.6+0.4\cos\delta \tag{A7}$$

Contrasting (A6) with (17), it is not difficult to find that the harmonic rotor fluxes in this fault case are relatively stronger in magnitude than the ones under the adjacent-phase open fault, which are responsible for the severe harmonic currents of Fig.24. Additionally, the Clarke and Park transformations for this non-adjacent-phase open fault can be referred to [17].

Under the *d-q* frame, the harmonic inductances of the energized phases, which are also associated with the third harmonic winding coils, can be represented by the followings:

$$\begin{bmatrix} \tilde{L}_d \\ \tilde{L}_q \end{bmatrix} \approx \eta_3 L_\theta \begin{bmatrix} -1.809\cos(2\theta+0.5\delta)+(0.691+0.4878\eta_3)\cos(4\theta+\delta) \\ -1.809\cos(2\theta-0.5\delta)-(0.691-0.4878\eta_3)\cos(4\theta+\delta) \end{bmatrix} \tag{A8}$$

Contrasting (A8) with (21), the harmonic inductances in this fault case are likewise stronger than the ones under the adjacent-phase open fault.

IX. References

[1] G. Liu, L. Liu, Q. Chen, and W. Zhao, "Torque Calculation of Five-Phase Interior Permanent Magnet Machine Using Improved Analytical Method," *IEEE Transactions on Energy Conversion*, vol. 34, no. 2, pp. 1023-1032, 2019.

[2] Y. Luo and C. Liu, "Multi-Vectors Based Model Predictive Torque Control for a Six-Phase PMSM Motor with Fixed Switching Frequency," *IEEE Transactions on Energy Conversion*, pp. 1-1, 2019.

[3] Q. Chen, W. Zhao, G. Liu, and Z. Lin, "Extension of Virtual-Signal-Injection-Based MTPA Control for Five-Phase IPMSM Into Fault-Tolerant Operation," *IEEE Transactions on Industrial Electronics*, vol. 66, no. 2, pp. 944-955, 2019.

[4] A. S. Abdel-Khalik, M. A. Elgenedy, S. Ahmed, and A. M. Massoud, "An Improved Fault-Tolerant Five-Phase Induction Machine Using a Combined Star/Pentagon Single Layer Stator Winding Connection," *IEEE Transactions on Industrial Electronics*, vol. 63, no. 1, pp. 618-628, 2016.

[5] Y. Sui, P. Zheng, Z. Yin, M. Wang, and C. Wang, "Open-Circuit Fault-Tolerant Control of Five-Phase PM Machine Based on Reconfiguring Maximum Round Magnetomotive Force," *IEEE Transactions on Industrial Electronics*, vol. 66, no. 1, pp. 48-59, 2019.

[6] A. Mohammadpour and L. Parsa, "Global Fault-Tolerant Control Technique for Multiphase Permanent-Magnet Machines," *IEEE Transactions on Industry Applications*, vol. 51, no. 1, pp. 178-186, 2015.

[7] E. B. Sedrine, J. Ojeda, M. Gabsi, and I. Slama-Belkhodja, "Fault-Tolerant Control Using the GA Optimization Considering the Reluctance Torque of a Five-Phase Flux Switching Machine," *IEEE Transactions on Energy Conversion*, vol. 30, no. 3, pp. 927-938, 2015.

[8] A. K. M. Arafat and S. Choi, "Optimal Phase Advance Under Fault-Tolerant Control of a Five-Phase Permanent Magnet Assisted Synchronous Reluctance Motor," *IEEE Transactions on Industrial Electronics*, vol. 65, no. 4, pp. 2915-2924, 2018.

[9] W. Huang, W. Hua, F. Chen, F. Yin, and J. Qi, "Model Predictive Current Control of Open-Circuit Fault-Tolerant Five-Phase Flux-Switching Permanent Magnet Motor Drives," *IEEE Journal of Emerging and Selected Topics in Power Electronics*, vol. 6, no. 4, pp. 1840-1849, 2018.

[10] G. Liu, Z. Lin, W. Zhao, Q. Chen, and G. Xu, "Third Harmonic Current Injection in Fault-Tolerant Five-Phase Permanent-Magnet Motor Drive," *IEEE Transactions on Power Electronics*, vol. 33, no. 8, pp. 6970-6979, 2018.

[11] H. Guzman *et al.*, "Comparative Study of Predictive and Resonant Controllers in Fault-Tolerant Five-Phase Induction Motor Drives," *IEEE Transactions on Industrial Electronics*, vol. 63, no. 1, pp. 606-617, 2016.

[12] A. Mohammadpour and L. Parsa, "A Unified Fault-Tolerant Current Control Approach for Five-Phase PM Motors With Trapezoidal Back EMF Under Different Stator Winding Connections," *IEEE Transactions on Power Electronics*, vol. 28, no. 7, pp. 3517-3527, 2013.

[13] H. Guzman, F. Barrero, and M. J. Duran, "IGBT-Gating Failure Effect on a Fault-Tolerant Predictive Current-Controlled Five-Phase Induction Motor Drive," *IEEE Transactions on Industrial Electronics*, vol. 62, no. 1, pp. 15-20, 2015.

[14] B. Tian, Q. An, J. Duan, D. Sun, L. Sun, and D. Semenov, "Decoupled Modeling and Nonlinear Speed Control for Five-Phase PM Motor Under Single-Phase Open Fault," *IEEE Transactions on Power Electronics*, vol. 32, no. 7, pp. 5473-5486, 2017.

[15] H. Zhou, W. Zhao, G. Liu, R. Cheng, and Y. Xie, "Remedial Field-Oriented Control of Five-Phase Fault-Tolerant Permanent-Magnet Motor by Using Reduced-Order Transformation Matrices," *IEEE Transactions on Industrial Electronics*, vol. 64, no. 1, pp. 169-178, 2017.

[16] L. Cheng, Y. Sui, P. Zheng, P. Wang, and F. Wu, "Implementation of Postfault Decoupling Vector Control and Mitigation of Current Ripple for Five-Phase Fault-Tolerant PM Machine Under Single-Phase Open-Circuit Fault," *IEEE Transactions on Power Electronics*, vol. 33, no. 10, pp. 8623-8636, 2018.

[17] B. Tian, Q. An, J. Duan, D. Semenov, D. Sun, and L. Sun, "Cancellation of Torque Ripples With FOC Strategy Under Two-Phase Failures of the Five-Phase PM Motor," *IEEE Transactions on Power Electronics*, vol. 32, no. 7, pp. 5459-5472, 2017.

[18] G. Liu, C. Song, and Q. Chen, "FCS-MPC-Based Fault-Tolerant Control of Five-Phase IPMSM for MTPA Operation," *IEEE Transactions on Power Electronics*, pp. 1-1, 2019.

[19] L. Zhang, Y. Fan, R. Cui, R. D. Lorenz, and M. Cheng, "Fault-Tolerant Direct Torque Control of Five-Phase FTFSCW-IPM Motor Based on Analogous Three-Phase SVPWM for Electric Vehicle Applications," *IEEE Transactions on Vehicular Technology*, vol. 67, no. 2, pp. 910-919, 2018.

[20] O. Dordevic, M. Jones, and E. Levi, "A Comparison of Carrier-Based and Space Vector PWM Techniques for Three-Level Five-Phase Voltage Source Inverters," *IEEE Transactions on Industrial Informatics*, vol. 9, no. 2, pp. 609-619, 2013.

[21] W. Zhao, B. Wu, Q. Chen, and J. Zhu, "Fault-Tolerant Direct Thrust Force Control for a Dual Inverter Fed Open-End Winding Linear Vernier Permanent-Magnet Motor Using Improved SVPWM," *IEEE Transactions on Industrial Electronics*, vol. 65, no. 9, pp. 7458-7467, 2018.

[22] Z. Keliang and W. Danwei, "Relationship between space-vector modulation and three-phase carrier-based PWM: a comprehensive analysis [three-phase inverters]," *IEEE Transactions on Industrial Electronics*, vol. 49, no. 1, pp. 186-196, 2002.

[23] O. L. Sanchez *et al.*, "Carrier-Based PWM Equivalent to Multilevel Multiphase Space Vector PWM Techniques," *IEEE Transactions on Industrial Electronics*, pp. 1-1, 2019.

[24] G. Liu, L. Qu, W. Zhao, Q. Chen, and Y. Xie, "Comparison of Two SVPWM Control Strategies of Five-Phase Fault-Tolerant Permanent-Magnet Motor," *IEEE Transactions on Power Electronics*, vol. 31, no. 9, pp. 6621-6630, 2016.

[25] Q. Chen, G. Liu, W. Zhao, L. Qu, and G. Xu, "Asymmetrical SVPWM Fault-Tolerant Control of Five-Phase PM Brushless Motors," *IEEE Transactions on Energy Conversion*, vol. 32, no. 1, pp. 12-22, 2017.

[26] O. Dordevic, E. Levi, and M. Jones, "A Vector Space Decomposition Based Space Vector PWM Algorithm for a Three-Level Seven-Phase Voltage Source Inverter," *IEEE Transactions on Power Electronics*, vol. 28, no. 2, pp. 637-649, 2013.

[27] L. Parsa and H. A. Toliyat, "Five-phase permanent-magnet motor drives," *IEEE Transactions on Industry Applications*, vol. 41, no. 1, pp. 30-37, 2005.

[28] R. Hyung-Min, K. Ji-Woong, and S. Seung-Ki, "Synchronous frame current control of multi-phase synchronous motor. Part I. Modeling and current control based on multiple d-q spaces concept under balanced condition," in *Conference Record of the 2004 IEEE Industry Applications Conference, 2004. 39th IAS Annual Meeting.*, 3-7 Oct. 2004 2004, vol. 1, pp. 1-63.

[29] B. Tian, G. Mirzaeva, Q. An, L. Sun, and D. Semenov, "Fault-Tolerant Control of a Five-Phase Permanent Magnet Synchronous Motor for Industry Applications," *IEEE Transactions on Industry Applications*, vol. 54, no. 4, pp. 3943-3952, 2018.

[30] R. Hyung-Min, K. Ji-Woong, and S. Seung-Ki, "Synchronous-frame current control of multiphase synchronous motor under asymmetric fault condition due to open phases," *IEEE Transactions on Industry Applications*, vol. 42, no. 4, pp. 1062-1070, 2006.

[31] M. J. Durán, J. Prieto, F. Barrero, J. A. Riveros, and H. Guzman, "Space-Vector PWM With Reduced Common-Mode Voltage for Five-Phase Induction Motor Drives," *IEEE Transactions on Industrial Electronics*, vol. 60, no. 10, pp. 4159-4168, 2013.

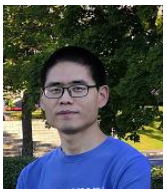

Bing Tian received the B.S. and M.S. degrees in electrical engineering from Harbin Engineering University, Harbin, China, in 2011 and 2013, respectively; and Ph.D. degree in electrical engineering from Harbin Institute of Technology, Harbin, China, in 2018. From 2018 to 2020, He was a postdoctoral fellow with Norwegian University of Science and Technology (NTNU), Trondheim, Norway, working on the electrification of offshore production system in close collaboration with Norwegian industry. His current research interests include fault-tolerant control of multi-phase drives, sensorless control of electric drives, neural network, quasi z-source inverter, sliding mode controller/observer, and repetitive control.

Marta Molinas (M'94) received the Diploma degree in electromechanical engineering from the National University of Asuncion, Asuncion, Paraguay, in 1992; the Master of Engineering degree from Ryukyu University, Japan, in 1997; and the Doctor of

Engineering degree from the Tokyo Institute of Technology, Tokyo, Japan, in 2000. She was a Guest Researcher with the University of Padova, Padova, Italy, during 1998. From 2004 to 2007, she was a Postdoctoral Researcher with the Norwegian University of Science and Technology (NTNU) and from 2008-2014 she has been professor at the Department of Electric Power Engineering at the same university. She is currently Professor at the Department of Engineering Cybernetics, NTNU. Her research interests include stability of power electronics systems, harmonics, instantaneous frequency, and non-stationary signals from the human and the machine. She is Associate Editor for the IEEE Journal JESTPE, IEEE PELS Transactions and Editor of the IEEE Transactions on Energy Conversion. Dr. Molinas has been an AdCom Member of the IEEE Power Electronics Society from 2009 to 2011.

Quntao An (S'10–M'11) received the B.S. degree in electrical engineering from Harbin University of Science and Technology, Harbin, China, in 2004, and the M.S. and Ph.D. degrees in electrical engineering from Harbin Institute of Technology, Harbin, China, in 2006 and 2011, respectively. From 2009 to 2010, he was an honorary fellow at Wisconsin Electric Machines and Power Electronics Consortium, University of Wisconsin-Madison. From 2009, he joined the faculty of Harbin Institute of Technology, and he is currently an Associate Professor. His research interests include electric machines and drives, power electronics, and energy storage technology.